Polyphenols as morphogenetic agents for the controlled synthesis of mesoporous silica nanoparticles

Jialuo Luo[a,b‡], Guido Panzarasa[a‡], Alina Osypova[a], Fabien Sorin[b], Fabrizio Spano[a], René M. Rossi[a], Amin Sadeghpour[a,c*], Luciano F. Boesel[a*]

[a] Empa, Swiss Federal Laboratories for Materials Science and Technology, Laboratory for Biomimetic Membranes and Textiles, Lerchenfeldstrasse 5, CH-9014, St.Gallen, Switzerland

[b] Laboratory of Photonic Materials and Fibre Devices (FIMAP), Institute of Materials, Ecole Polytechnique Fédérale de Lausanne (EPFL), CH-1015, Lausanne, Switzerland

[c] Empa, Swiss Federal Laboratories for Materials Science and Technology, Center for X-ray Analytics, Lerchenfeldstrasse 5, CH-9014, St.Gallen, Switzerland

ABSTRACT: Non-surfactant-induced synthesis of mesoporous silica nanoparticles (MSNP) are gaining increasing interest owing to their low toxicity and simple purification compared to conventional surfactant-based methods. Tannic acid (TA), considered as a glucose-derived polyphenol, was first employed a few years ago and has attracted great research interest. Despite recent progress, the mechanisms resulting in the porous structure remain to be elucidated. In this work, we have applied a sol-gel method to synthesize MSNPs using TA. Electron microscopy, dynamic light scattering (DLS), nitrogen adsorption and desorption (BET) method, small angle X-ray scattering (SAXS), and thermogravimetric analysis (TGA) are employed to characterize the resulting particles. The size, morphology and porosity of the resulting MSNPs can be tuned by varying the amount of TA. In addition, we have employed four structurally related polyphenols (gallic acid, ethyl gallate, eudesmic acid and quercetin) and compared their behaviour with TA in obtaining mesoporous particles. Our results help unravel the mechanisms of particle formation, specifically that the pKa values and supramolecular structure of the templates may be accounted for the particle size and pore formation, respectively.

INTRODUCTION

Mesoporous silica nanoparticles (MSNPs) have been the subject of intense investigation for potential use in catalysis, separation, or biomedicine thanks to their large surface area-to-volume ratios, tunable pore sizes as well as the variety of possible surface modification approaches that they allow. These properties make MSNPs highly attractive also for biomedical applications, especially for the development of multimodal imaging systems, controlled delivery[1] and sensing[2]. Surfactant-templating is the most widely used approach for the synthesis of mesoporous silica nanoparticles. In 1992 it was shown[3] that the self-assembly of surfactant molecules, when conducted in aqueous solutions of silica species, can result in spontaneous co-assembly of silica-surfactant mesophases. Removal of the surfactant leaves behind periodic mesoporous solids, the negative replica of the supramolecular assembly of the surfactant. Over the past years, a wide compositional range of mesoporous solids was produced[4], and the possibility to tune the pore sizes from one to tens of nanometers was demonstrated by using a variety of surfactants. In this regard, MCM-41 and SBA-15 (Mobil Composition of Matter no. 41 and Santa Barbara Amor-

phous no. 15, respectively) are excellent examples of the power of this approach.[5] However, the presence of residual surfactants in MSNPs constitutes one major drawback for their use in biomedical applications, as the most commonly used surfactants, including cetyltrimethylammonium bromide (CTAB), are cytotoxic. Therefore, extensive purification is necessary before the particles could be used for biological applications. The strong retention of surfactants makes their removal a difficult and time-consuming step, especially if performed by wet methods[6], or requires the calcination of the particles at high temperature, which in some cases can lead to the partial or total collapse of the internal porous structure[7].

In nature, the most striking examples of surfactant-templating strategy are provided by diatoms[8] and radiolarian[9], which show highly complex architectures carved in silica. These structures are formed by biomineralization, a templated self-assembly process in which preorganized organic surfaces regulate the nucleation, growth, morphology and orientation of inorganic crystals. To date, a variety of synthetic pathways have been proposed to mimic biomineralization, started from the early report of Dickey[10], who used an azo-dye (methyl orange) for the

synthesis of templated silica gels. The use of non-surfactants as templating agents was rediscovered decades later, when Wei *et al.* showed how monolithic mesoporous silica could be produced using D-glucose, dibenzoyl-L-tartaric acid, and D-maltose.[11] Subsequent studies indicated that other molecules, such as poly(propylene)imine dendrimers[12], organic hydroxycarboxylic acids[13] (including citric acid, lactic acid, malic acid and tartaric acid), β-cyclodextrin–urea complexes[14], fatty alcohols[15] and sugars[16] (including sucrose and fructose) could be successfully used to generate mesoporous silica monoliths. Such approach has then been successfully extended to the synthesis of nanoparticles. However, while the size of non-surfactant–templated MSNPs can be varied in a broad range without loss of monodispersity, the pore size is usually less than 4 nm due to the small size of the templating molecules.[16] Recently, Gao *et al.* proposed tannic acid[17] as an especially suitable non-surfactant for the synthesis of large-pore mesoporous silica nanoparticles.

Tannic acid (TA, decagalloyl glucose) is a type of water-soluble natural polyphenol derivative of glucose and the simplest tannin. TA is highly biocompatible and its medical uses are widespread thanks to its antibacterial and antioxidant properties.[17] Despite a growing interest[18] for tannic acid-templated MSNPs, however, the templating mechanism still remains unclear. It is generally hypothesized that the formation of the porous silica framework would be the result of hydrogen bonding interactions between TA (also in the form of supramolecular complexes) and silicate species originated from the hydrolysis of the organosilane precursor.[17] However, no systematic attempt has been reported to date to investigate this mechanism.

In the present work, we studied the influence of TA concentration on the size, porosity and morphology of MSNPs. We show that particle morphology can evolve from non-porous particles to hollow porous particles. To further explore the morphogenetic process, we also studied the effect of other polyphenols (gallic acid, ethyl gallate, eudesmic acid and quercetin). We demonstrate for the first time the possibility of varying the particle morphology in addition to the porosity. We show how the use of different polyphenols affects MSNPs morphology, specifically that the pKa values and supramolecular structure of templates are responsible for the particle size and pore formation, respectively.

EXPERIMENTAL

Materials

Concentrated (28%) ammonium hydroxide, tetraethoxysilane (TEOS), ethanol (absolute), tannic acid (TA), gallic acid (GA), ethyl gallate (EG), eudesmic acid (EA), quercetin (QU), concentrated (98%) sulfuric acid and concentrated (30%) hydrogen peroxide were purchased from Sigma-Aldrich and used as received. MilliQ water (resistivity ≥ 18 MΩ cm^{-1}) was thoroughly used.

Synthesis of non-porous silica nanoparticles

In a typical synthesis, 8 mL of concentrated ammonium hydroxide were diluted with 33 mL of water; ethanol was then added to a final volume of 320 mL. The solution's temperature was stabilized at 30°C under stirring; afterwards 2 mL of TEOS were added at once. Six hours after the addition of TEOS, the suspension was centrifuged (7800 rpm, 10 min) and the pellet was redispersed in ethanol to remove excess reactants. This cycle was repeated three times. Eventually, the particles were dispersed in ethanol.

Synthesis of porous silica nanoparticles

For the synthesis of porous silica nanoparticles, the selected templating agent was dissolved in 150 mL of ethanol and then added to the ammonia-water mixture. The procedure was then carried out as described for the synthesis of non-porous silica nanoparticles. Five different templating agents (TA, GA, EG, EA, QU) were used with different amounts (512 mg, 384mg, 256 mg, 128 mg and 64 mg in total). After synthesis, the particles were collected by centrifugation and were thoroughly washed by several cycles of centrifugation and redispersion in ethanol and water. Removal of organic residues by means of acid piranha treatment was performed for all particles. About 0.1g of particles were dispersed in water three times to exchange all the ethanol and the resulting aqueous suspension was treated with a diluted acid piranha solution (2 M H_2SO_4 and 10% H_2O_2) at 60°C for 2 h under stirring. The suspension was then centrifuged (7800 rpm, 10 min) and the procedure repeated. Eventually the particles were washed three times with water to get rid of acid residues and were redispersed in water.

Characterization

Scanning electron microscopy (SEM) was performed using a JEOL Hitachi S-4800. To facilitate imaging, a small drop of dilute ethanolic particle suspension was allowed to evaporate on a piranha-cleaned silicon substrate mounted on conductive tape and was then sputter-coated with 5 nm of Au-Pd alloy. Transmission electron microscopy (TEM) was performed using a JEOL JEM 2200fs. The samples were mounted on carbon-coated grids by evaporating a dilute particle suspension in ethanol. Dynamic light scattering (DLS) was performed to measure the hydrodynamic size as well as the polydispersity index (PdI) of the resulting particles using a Malvern Zetasizer Nano. All solutions were prepared in MilliQ water. Thermogravimetric analysis (TGA) was performed with as-prepared particles. The particles were directly centrifuged out and dried at 50°C overnight without washing step. About 10 mg of the resulting samples were then filled into an Al_2O_3 pan and heated from 25°C to 900°C with an increasing rate of 20°C min^{-1} under oxidant conditions (50 mL min^{-1} of synthetic air made of 80% nitrogen and 20% oxygen). Nitrogen sorption measurements were used to determine the surface area and pore volume of the silica particles. The particles were dried first at 50°C overnight and then at 80°C for 1200 minutes before the introduction of N_2 gas. The nitrogen adsorption/desorption cycles were measured at 77 K using a Micromeritics Triflex. The

Brunauer–Emmet–Teller (BET) method was used to calculate the specific surface area. The pore volume was obtained from analysis of the adsorption branch using the Barrett–Joyner–Halenda (BJH) method. Atomic force microscopy (AFM) analysis was carried out using a scanning probe microscope Nanosurf FlexAFM V5 equipped with a C3000 controller. The ethanoic dispersion of non-templated silica nanoparticles and GA-templated MSNPs was deposited on clean glass wafer and dried in ambient condition. The dry sample was scanned in tapping mode with a silicon probe (Tap SHR300, a high resolution cantilever with a sharp diamond-like carbon tip having a precise radius of 1 nm, Budget Sensor) with a resonance frequency of 300 kHz and a force constant of 40 N/m. The image analysis was processed with Gwyddion software (version 2.51).

Small-angle X-ray scattering (SAXS) studies were further performed in order to evaluate the particles pore sizes and their surface roughness. A Nanostar SAXS instrument (Bruker GmbH, Karlsruhe, Germany), with a microfocused X-ray source (Incoatec GmbH, Geesthacht, Germany), generating Cu Kα radiation with a wavelength of 0.154 nm, has been used. The system is equipped with MONTEL optics (two Göbel mirrors arranged perpendicular to each other) and two pinholes of 300 μm to focus the X-ray beam and a VÅNTEC-2000, Xe-based gas avalanche detector capable of photon counting with 0.5 seconds temporal resolution. By applying a sample-detector distance of ~107 cm, a q_{min} of 0.06 nm⁻¹ could be accessible where $q = \frac{4\pi}{\lambda}\sin(\theta)$ and 2θ is the scattering angle. This corresponds to a maximum spatial resolution of 52.4 nm. All the experiments were carried out in a vacuum chamber (0.01 mbar) and at the room temperature over 2 hours of exposure time. Although the electron density contrast of the analyzed particles (silica) with respect to solvent (water) is quite high, a long exposure time was still needed in order to reveal scattering features from pores within the particles. The samples were transferred into quartz capillaries of 1.5 mm in outer diameter (Hilgenberg GmbH, Malsfeld, Germany). The capillaries were vacuum tightened using sealing wax. The scattering profiles of empty and water filled capillaries were obtained under the same conditions and a semi-transparent beam stop enabled to perform normalization of the curves and then background noise subtraction.

RESULTS AND DISCUSSION

Effect of tannic acid concentration on the morphology of mesoporous silica nanoparticles

Synthesis of silica nanoparticles by the sol-gel Stöber method involves the controlled hydrolysis and condensation of tetraethoxysilane in alcohol-water mixtures in presence of ammonia as basic catalyst. This approach leads to non-porous nanoparticles unless suitable templating agents are used. Here, we resorted to a previously optimized protocol[19] for the synthesis of 100 nm-diameter non-porous silica nanoparticles to study the morphogenetic properties of TA and other related polyphenols.

The complete solubilization of all components is of great importance to achieve control on particle nucleation and growth. Solubility tests were performed in order to determine the upper limit concentration of TA, which, for our reaction system, was determined to be about 1.6 mg.mL⁻¹ (corresponding to 512 mg in total of TA). The total amount in mg of the templating agent used for each synthesis was used as reference to identify the samples.

Dynamic light scattering (DLS) and scanning electron microscopy (SEM) were employed for the determination of average diameter and polydispersity of the resulting particles. The results show that the addition of 64 mg of TA resulted in a slight increase in the particle diameter compared to non-mesoporous nanoparticles (blank) (Table 1). The size of TA512-MSNP measured through SEM images should be taken into consideration with caution due to the irregular morphology. We have presented here the diameter of both long axis and short axis. The effective particle size should be located between the two values. Of note, the particle size determined by DLS is in this case equivalent to that of the long axis. Except for this case (TA512), we noticed that the particle size grows only slightly with the increase in the TA content. Moreover, all samples show a narrow, monodisperse distribution (PdI < 0.1). The SEM provided also preliminary information about particle morphology, which experienced a change from spherical to irregular (cauliflower-like), visible for MSNPs prepared with 256mg or 512mg of TA (Figure 1, left column). Moreover, from the SEM images, we inferred that the irregular particles obtained with 512mg were hollow. Both findings are likely to originate from the aggregation of small sub-particles. TEM shows an increasingly porous structure in the particles for increasing amounts of TA (Figure 1, right column).

Table 1. Size information (obtained from DLS and SEM) of resulting particles templated with TA

Sample	Particle size, DLS (nm)	PdI from DLS	Particle size, SEM (nm)
Blank SNP	157	0.027	122±20
TA64-MSNP	155	0.014	145±17
TA128-MSNP	170	0.026	146±18
TA256-MSNP	175	0.012	150±28
TA384-MSNP	167	0.033	152±23
TA512-MSNP	225	0.080	222±37 (long axis) 156±23 (short axis)

In contrast with previous literature reports[17, 18c], we noticed that a certain amount of TA was retained inside the silica matrix even after several cycles of washing with ethanol and water, as the particles were of a light-brown color. The removal of residual templating agent ("detemplating") from mesoporous silica nanoparticles is usually accomplished by both dry and wet methods. The most conventional treatment is calcination, *i.e.* particles are

subjected to high temperature (typically 500-600 °C) in an oxidizing atmosphere to burn the residues of organic templating agents. However, this approach can lead to particle sintering, with consequent worsening of colloidal stability, and damage of the porous structure (*e.g.* pore collapsing)[20]. Milder detemplation approaches are based on wet processes such as ion exchange (for ionic surfactants) or, chemical degradation by means of Fenton-like reactions and acid piranha solution (for non-ionic species)[21]. Here, we studied the removal of residual TA by means of calcination as well as of acid piranha treatment (refer to the experimental section for details). Both approaches resulted in white particles (Figure S2a) and electron microscopy analysis (SEM and TEM) showed that the particle morphology was not affected by any of the treatments (Figure S2b). However, from a qualitative point of view, calcination was found to affect more the colloidal stability of the particles compared to the piranha treatment, which produced stable suspensions.
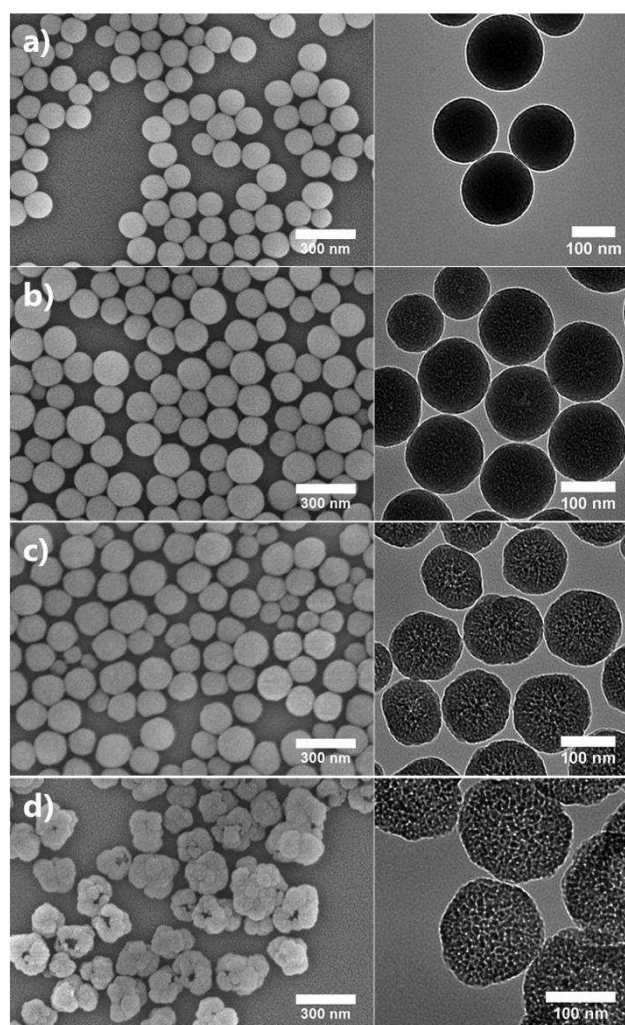

Figure 1. SEM (left column) and TEM (right column) images of TA-templated silica nanoparticles prepared with increasing amounts of templating agent: a) TA64-MSNP, b) TA128-MSNP, c) TA256-MSNP, d) TA512-MSNP.

To investigate more in detail the morphology and especially the porosity of the particles, SAXS measurements were performed on samples before and after detemplation with piranha treatment. In Figure 2a, the intensity versus scattering vector, q, from non-porous silica particles is shown. The 1D scattering profile has been obtained from azimuthal integration of the 2D pattern represented in the inset of Figure 2a. First of all, the Porod slope of -4.0 reveals the existence of a smooth particle surface which is expected to be the case for non-porous particles. In addition, the nanoparticle size can usually be estimated using the Guinier approximation[22]. However, as the particles size (~200 nm) in this study went beyond the observation window of our SAXS setup, the Guinier region of the scattering curve was not accessible. Nevertheless, it is known that, the oscillations (observation of minima/maxima) in the scattering form factor of spheres are indication for system monodispersity. It is important to note that, the observed minima position in equidistant intervals, with the first minimum at $4.5/R_g$ (R_g is the radius of gyration and, for a sphere and is related to nominal radius, r, of spherical particle by $R_g = \left(\sqrt{3/5} \cdot r \right)$). As the size distribution of particles becomes broader these oscillations are suppressed and for highly polydisperse sample, a smooth decay in the scattering intensity will be recorded. In our studied non-templated silica particles system, the maxima and minima could still be resolved in the scattering intensity (see the arrow around 0.085 nm^{-1} in Figure 2a), though the order of this minimum could not be determined solely from SAXS data.[23] Here, we referred to primary knowledge on size estimation from DLS. For particles of radius around 100 nm, the first minimum position is approximated around ~0.045 nm^{-1}. This would mean that the minimum observed around 0.085 nm^{-1} must correspond to the second minima as indicated in the Figure 2a. Having this in mind, we further implemented the indirect Fourier transformation (IFT)[24], considering the r_{max} of 200 nm, to simulate the scattering pattern while precisely extrapolating the curve to ultra-small angles. The IFT calculation was implemented using the GIFT software (University of Graz, Austria). The simulated curve in reciprocal space corresponds to the pair-distance distribution function (also called $p(r)$ function), in real space which reveals detailed information on the size and shape of the particles. The $p(r)$, shown in Figure 2b, corresponds to R_g value of 65.7 ±2 nm and has fairly symmetric shape which is normally associated with low polydispersity in spherical particles systems.. However, a quantitative measure of polydispersity index requires high resolution data at ultra-small angle regime for this system.

We also performed the classical Porod analysis in order to evaluate surface roughness of the synthesized particles. In this approach, the decay rate of the intensity versus q in log-log scale, is calculated. The slope of -4, typically corresponds to scattering from particles of smooth surface while deviation from that, indicates surface roughness. In our studied systems, the Porod values vary from -4 (non-templated nanoparticles) to -3.4 (for templated nanoparticles with the highest applied TA concentration). Therefore, the comparison of the Porod slope values for different particles shows that the later displays higher

surface roughness with respect to the former one (Figure 3a,c,e and Figure 4b), in agreement with the morphologies observed by electron microscopy[25]. This monotonous and systematic decrease in Porod slope with increasing amounts of TA indicates well controlled surface roughness through this synthetic approach.
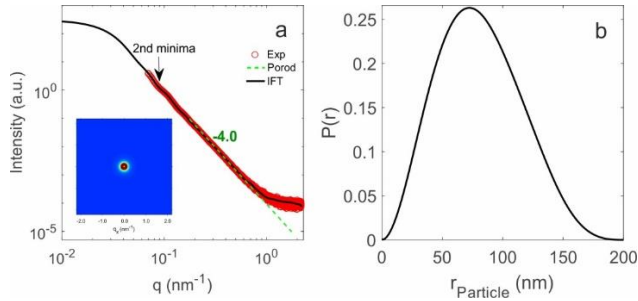

Figure 2. a) Experimental and simulated scattering intensities versus scattering vector from silica particles synthesised without templating agent. The inset represents the 2D scattering pattern. b) the corresponding $p(r)$ obtained from IFT calculation.

The X-ray scattering from templated nanoparticles with varying amounts of TA demonstrates an additional feature; a hump at around 0.5 to 1 nm^{-1}, depending on the templating agent concentration. The hump is a typical scattering feature from porous materials which originates from the electron density variations within the particles and its position and intensity is correlated with the pore size and the total number of pores[26]. In order to carefully analyze the pores within the particles, we subtracted the fitted Porod line from the experimental data within the q-range of observation of the hump. The resulting curve, so called residual scattering, was further considered as the new pattern, its IFT analysis revealed the $P(r)$ function of the pores (see Figure 3b,d,f). The radius of gyration obtained from this approach shows an increase in the pore radius from about 2 nm in TA128-MSNP to about 3.5 nm in TA512-MNSP (Figure 4a). The evaluated pore sizes, similar to the particles surface roughness, increase with concentration of templating agent. It is also interesting to figure out that nearly identical scattering profiles have been acquired from particles before and after removal of templates by piranha treatment; the calculated Porod slopes and the radii of gyration of the pores vary only within the margin of error (see Figure 4b), suggesting that piranha treatment has no effect on both pore size and roughness of the particles.

Complementary information about porosity was obtained by means of nitrogen sorption-desorption measurements, which were carried out on detempled samples (Figure 5). The resulting BET surface area and pore volume values, summarized in Table 3, were found to increase with the amount of TA used. The particles obtained with the two lowest amounts of templating agent (TA64-MSNP and TA128-MSNP) displayed a very low nitrogen sorption, suggesting a non-porous structure. The nitrogen sorption is nearly zero in a pressure range lower than 0.8 P/P$_o$, which may imply that the adsorption mainly happened on the particle surface. In contrast, the isotherms of TA256-MSNP were characterized by a type IV curve with a dominant type H2 hysteresis loop between 0.4 P/P$_o$ and 0.8P/P$_o$, strongly indicating the presence of mesopores. The hysteresis loop at about 0.9 P/P$_o$ can be attributed to interconnected pores. This latter feature is shared with the TA512-MSNP, of which the long hysteresis loop between 0.4 P/P$_o$ and 0.9 P/P$_o$ may suggest the presence of different populations of pores.
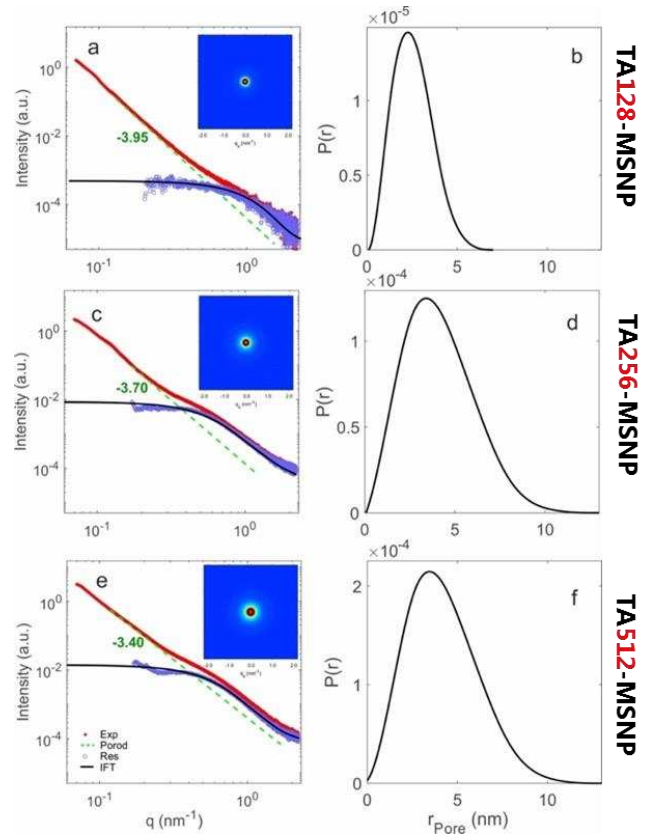

Figure 3. a, c and e) The experimental scattering patterns and their relevant residual scattering obtained from subtraction of Porod line are shown together with the IFT evaluation of residual scattering. The insets represent the 2D scattering patterns. b, d and f) the pair-distance distribution function, $p(r)$, obtained from IFT analysis of residual scattering from pores. The distribution reveals increase in pore size and pore volume by increasing templating agent concentration, in this case TA.

The molecular dimensions of a tannic acid molecule are 1.85nm × 1.65nm × 1.01 nm[27], which would correspond to a volume of around 3 nm^3. On the basis of SAXS and BET results, however, it is reasonable to conclude that the pore size in our TA-templated MSNPs is larger than the size of a single TA molecule. This is in accordance with the suggestion of Gao[17] that TA could self-assemble into supramolecular structures, most probably by means of hydrogen bonding, which would then direct the pore formation. However, our results suggest also that there could be a critical concentration of TA, below which a porous structure could not be achieved (*e.g.* because of insufficient degree of self-assembly) or, conversely, above

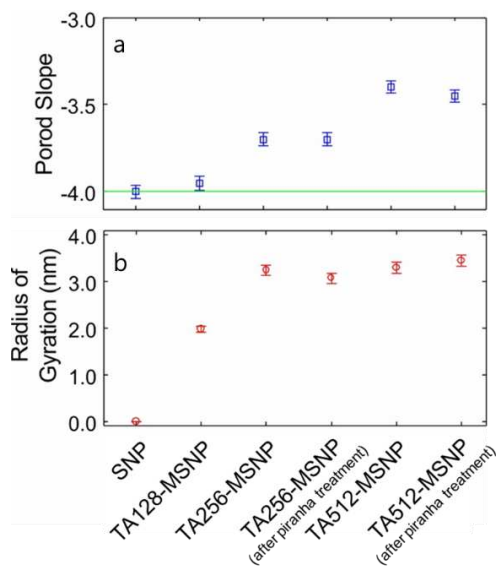which would result in a morphological change (see TA256- and TA512-MSNP).

Figure 4. Radius of gyration (Rg) of the pores and the Porod slope values obtained from TA-templated silica nanoparticles before and after piranha treatment.

Particles	Surface area (m²/g)	Pore volume (cm³/g)	Pore size by SAXS (nm)
TA64-MSNP	26.0	0.27	-
TA128-MSNP	27.4	0.24	5.2±0.2
TA256-MSNP	255.2	0.52	8.4±0.2
TA512-MSNP	362.9	1.10	8.6±0.2
GA64-MSNP	25.5	0.14	-
GA128-MSNP	11.2	0.03	-
GA256-MSNP	103.1	0.01	-
GA512-MSNP	99.7	0.05	-

Table 2. Structural properties of TA-templated particles as determined by BET and SAXS

EM images show the change in particle porosity and morphology under different concentrations of TA. Pore size increases with the content of TA, which is in agreement with SAXS results with an increase of radius of gyration from 2 nm to 3.5 nm corresponding to a pore size from 5 nm to 9 nm. However, comparing the SAXS and BET results of TA256- and TA512-MSNP samples, it is clear that the surface area is not accompanied by an increase of pore size. This may imply that the increase of surface area does not come from the enlargement of single pores but is mainly due to the interconnection between pores or the presence of cracks in the particles, which are supported by the nitrogen adsorption and desorption isotherm of TA512-MSNP. In addition, the morphology of the mesoporous nanoparticles changes: under higher concentrations of TA, particles with irregular shapes were formed. The particles showed no longer a

particulate and smooth surface as at lower concentrations of TA, instead, irregular shape and rough surface were formed. This observation is consistent with the conclusion from SAXS, which points out that surface roughness gradually increased from TA128 to TA512. Moreover, it is also interesting to see that the TA512-MSNP have a cauliflower shape, very likely to originate from the aggregation of small sub-particles (see discussion on SEM/TEM results). The morphology change could be interpreted according to the mechanism of particle formation. It is generally agreed that in sol-gel process the silica precursors are hydrolyzed and form small nuclei which are considered as primary particles. The primary particles will further aggregate to form the large particles.[28] When TA is used as template, the silica moieties can form hydrogen bonds with TA and associate around TA. But due to the irregular shape of TA itself and the TA supramolecular network, the primary particles formed are also irregular. Such primary particles can hardly pack as densely as spherical ones to form a uniform structure, but in contrary may result in cracks between connected primary particles and an irregular morphology of the final particles. The information from EM images and BET as well as SAXS results all support this hypothesis.
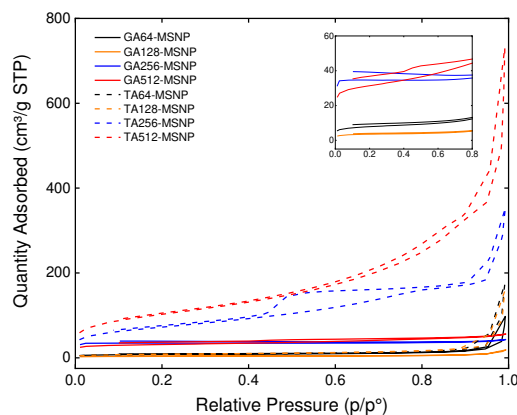

Figure 5. Nitrogen adsorption-desorption isotherms of templated MSNPs after detemplation.

Investigation of tannic acid-related polyphenols as morphogenetic agents

One possible explanation for the pore formation, as suggested by a previous study[17], is that the mesopores can be attributed to the formation of TA supramolecular network. However, no study has been carried out so far to verify this hypothesis. To further unravel the morphogenetic properties of TA, we focused on strictly related molecules, namely: gallic acid, ethyl gallate, eudesmic acid and quercetin with their chemical structure presented below (Figure 6).

Tannic acid is decagalloyl glucose, thus GA can be considered as its monomer. When the synthesis of silica nanoparticles was carried out by substituting TA with GA, particle size increased (from about 240 nm to about 600 nm) as a function of the GA amount with other reaction

conditions being constant (Figure 7 and S3). Moreover, the resulting particles were of a dark-brown color, which was not altered after prolonged washings with ethanol and water. Even repeated treatments with piranha solution were only partially effective in bleaching the color, suggesting that a fraction of the templating agent was still buried in the particles. Colorless particles could be obtained only by means of calcination. This dark-brown color is hypothesized to be the result of GA polymerization, as it is known that polyphenols can undergo polymerization in alkaline environments in presence of air with formation of brown-colored products.[29] EG and EA were also used under the same conditions, resulting in white particles with a similar trend in the increase of particle size upon increasing amounts of templating agents: 233 nm to 490 nm for EG and 240 nm to 731 nm for EA (Figure 7 and S3). When QU was chosen as templating agents, particles were slightly yellow and the growth was similar to that obtained with EG. The results of DLS and SEM are summarized in Table S1 and the particle size evolution is compared in Figure 7.
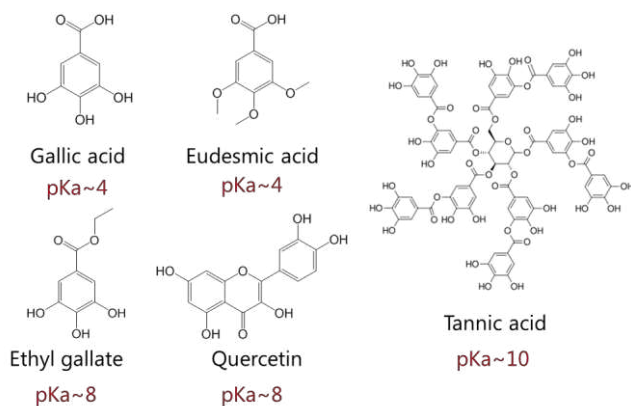

Figure 6. Chemical structure and respective acidity constants of polyphenols used as morphogenetic agents

The presence of functional group moieties seems to play an important role for particle growth, as is apparent from comparing the results of Figure 7 with Figure 6. The pH of the reaction mixture may be a parameter that could explain the growth and the final size of Stöber silica particles. In a Stöber reaction, the base is added as a catalyst to facilitate the hydrolysis. At a high pH, more hydroxide ions are present in the system that can directly attack the silica atoms in the silica source (e.g. TEOS) through a nucleophilic mechanism, which leads to a faster hydrolysis of the silica precursors, contributing to a larger particle size. However, if the hydrolysis is fast at the initial nucleation step, then more nuclei will be generated so that the final particle size may be smaller. In our case, the five templates exhibit a pKa value of ~4 for GA[30] and EA[31], ~8 for EG and QU[32] and ~10 for TA[17], which decreases the pH of the reaction mixture at different extents. When having the same weight dosage, templates with lower pKa value will consume more base catalyst. The initial silica nucleation process is constrained, thus fewer nuclei are generated and result in bigger particles. This helps explain the bigger particle size in the case of template-

induced particles comparing to the blank silica nanoparticles. Our results suggest that the nucleation process is more dominant for the final particle size compared to the particles growth speed. Furthermore, as more templates are added, the amount of ammonium ions consumed through the reaction with templates will increase, hindering the hydrolysis of silica precursors to form fewer nuclei at the beginning. Thus, bigger particles are generated.
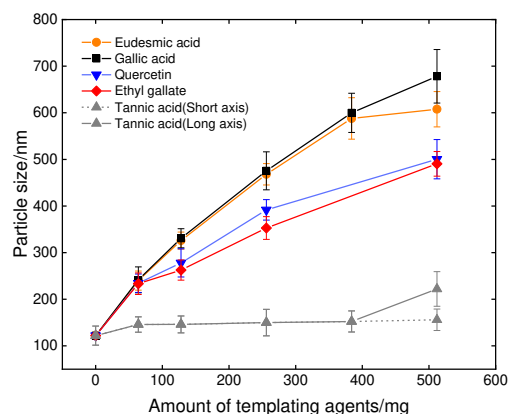

Figure 7. Size of particles out of various templating agents as a function of mass of templating agent.

In addition to the difference in size, there are differences in pore formation as well. Pores are only found in particles templated by GA and TA. We attributed this to the existing state of the templates in the mixture. To verify this hypothesis, we have performed DLS measurements for the reaction mixture prepared using the same procedure but without silica precursors (Table S2). The results showed that only at the highest concentration (512mg) the TA and GA molecules assembled to stable aggregates or supramolecular structure. The size of TA aggregates remained almost constant with time while GA aggregates kept growing. On the contrary, EA, EG and QU did not show any tendency to form stable aggregates. This explains the role of the polyphenols in the synthesis. Likely, the ones forming a stable network are capable to lead to porous structure. The size of aggregates by DLS roughly corresponds to the size of the particles, not to the pore sizes. According to this, we speculate that the mesoporous structure is a consequence of the crosslinking of silica precursors in the free space of the TA and GA aggregates, and therefore the pores should be interconnected, which is in accordance with the BET and TEM of TA. For GA, we have not noticed an interconnected pore structure but instead, shallow holes and gully appeared on the surface (Figure 8), very likely sculptured by the GA polymer chains. The AFM and SEM images indicate a very different morphology of the particles between the well-templated MSNPs (e.g. GA MSNPs) and the poorly-templated (e.g. EG particles) as well as non-templated ones. When GA was dissolved in the reaction mixture for a longer time before the addition of TEOS, bigger parti-

cles were obtained, which further support the hypothesis of pore formation (Figure S4).

To verify the decisive influence of supramolecular structure towards the pore formation, we quantified the mass loss of the particles after calcination resulting from all five templates at different concentrations (Table 3). The SNP samples, used as a contrast, were calcinated to measure the mass loss originated from the silica substance. Then, the mass loss of the templated ones was measured. The difference of the mass loss between the templated ones and the SNP samples was considered as the net weight of the templates contained in the particles.
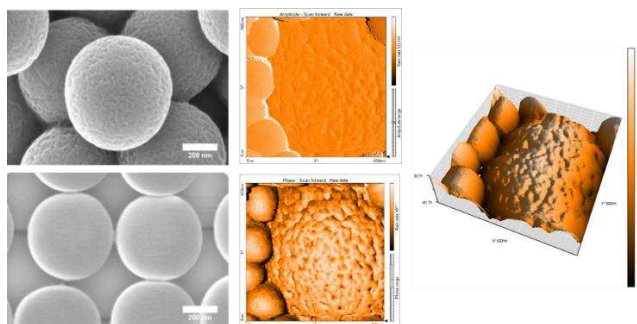

Figure 8. Comparison of particle surface. Left: SEM images of particles templated by GA (top) and EG (bottom). Center: AFM images of one GA512-MSNP particle (rough) surrounded by smooth, non-templated SNP particles. Right: AFM 3D reconstruction of the same particles.

The non-templated SNP samples showed a mass loss of 10.3% which could be attributed to the incomplete reactions and bounded water molecules on the surface. The mass loss of all detemplated samples fell within 2% of this value, indicating a relatively complete removal of templating agents, except for GA512. In this case, the mass loss was slightly higher, showing that GA was buried inside particles. This could suggest the formation of closed pores.

Regarding the as-synthesized samples, the TA and GA samples showed an increase of mass loss with the amount of templates, while the mass loss of the EA, EG, and QU samples remained relatively stable. It implies that, for EA, EG, and QU samples, the polyphenols were not surrounded by TEOS and had no templating effect for the pore formation. Thus, the introduction of EA, EG, and QU did not lead to porous structure but only slowed down the hydrolysis of the silica precursors to generate fewer nuclei and give a larger particle size. The extra mass loss compared to the blank SNPs contrast is attributed to the attached polyphenols on the surface. On the contrary, TA and GA are shown to be templates by the increase of remained weight with the initial concentration, demonstrating the participation of TA and GA in the pore formation. Moreover, a larger mass loss is associated with a higher porosity, in agreement with the BET results.

Table 3. Mass loss before and after calcination of particles prepared with different morphogenetic agents

Sample name	Mass loss (%), detemplated	Mass loss (%), as-synthesized
SNP	10.3	-
TA64-MSNP	9.0	10.5
TA128-MSNP	11.8±1.6	11.5±0.4
TA256-MSNP	8.5	20.5
TA512-MSNP	10.3±0.6	39.9±0.8
GA64-MSNP	9.8	10.8
GA128-MSNP	12.2±1.8	11.9±0.08
GA256-MSNP	10.2	14.2
GA512-MSNP	12.5±2.1	19.0±0.2
EG64-MSNP	9.3	11.4
EG128-MSNP	9.7	11.3
EG256-MSNP	8.1	11.5
EG512-MSNP	11.6±2.4	11.5±0.4
EA64-MSNP	9.3	10.8
EA128-MSNP	9.4	11.3
EA256-MSNP	9.4	11.4
EA512-MSNP	11.9±2.4	11.0±0.8
QU64-MSNP	9.6	11.0
QU128-MSNP	9.8	10.8
QU256-MSNP	9.8	11.1
QU512-MSNP	9.8	11.6

CONCLUSION

Mesoporous silica nanoparticles have been successfully synthesized using TA as morphogenetic agent. Piranha treatments were used to a complete removal of TA. We managed to control the size, morphology and porosity of the resulting MSNPs by varying the amount of TA. Tannic acid and four related polyphenols (GA, EG, EA, QU) were employed in attempt to unravel the formation mechanism of MSNP by TA. The results showed that only TA and GA lead to porous structure. This observation agrees with TGA results that only MSNPs produced with these templating agents have an increasing mass loss along with the concentration, which indicates their participation in the synthesis as templating agents. Mass loss from TGA results, combined with DLS measurements, indicated the formation of big aggregates, which should be responsible for the porous morphology. The involved polyphenols have different impact on the size of final particles: this was determined by the pKa of the polyphenols. Our work suggests a new direction to study the morphogenetic mechanism of polyphenols on the synthesis of mesoporous particle structure, with potential opportunities for drug delivery and other bio-related applications.

ASSOCIATED CONTENT

Supporting Information. SEM, TEM and photographical images of the non-porous and mesoporous particles. Particle size (by SEM and DLS) of all prepared particles. This material

is available free of charge via the Internet at http://pubs.acs.org.

AUTHOR INFORMATION

Corresponding Authors

* Amin Sadeghpour: Amin.Sadeghpour@empa.ch, Luciano F. Boesel: luciano.boesel@empa.ch

Present Addresses

†If an author's address is different than the one given in the affiliation line, this information may be included here.

Author Contributions

The manuscript was written through contributions of all authors. / All authors have given approval to the final version of the manuscript. / ‡These authors contributed equally.

ABBREVIATIONS

CCR2, CC chemokine receptor 2; CCL2, CC chemokine ligand 2; CCR5, CC chemokine receptor 5; TLC, thin layer chromatography.

REFERENCES

1. Zhang, Q.; Liu, F.; Nguyen, K. T.; Ma, X.; Wang, X.; Xing, B.; Zhao, Y., Multifunctional Mesoporous Silica Nanoparticles for Cancer-Targeted and Controlled Drug Delivery. *Advanced Functional Materials* **2012**, *22*, 5144-5156.

2. Widmer, S.; Reber, M. J.; Muller, P.; Housecroft, C. E.; Constable, E. C.; Rossi, R. M.; Bruhwiler, D.; Scherer, L. J.; Boesel, L. F., Incorporation of a FRET dye pair into mesoporous materials: a comparison of fluorescence spectra, FRET activity and dye accessibility. *Analyst* **2015**, *140*, 5324-5334.

3. Kresge, C. T.; Leonowicz, M. E.; Roth, W. J.; Vartuli, J. C.; Beck, J. S., Ordered mesoporous molecular sieves synthesized by a liquid-crystal template mechanism. *Nature* **1992**, *359*, 710-712.

4. (a) Stevens, W. J. J.; Lebeau, K.; Mertens, M.; Van Tendeloo, G.; Cool, P.; Vansant, E. F., Investigation of the Morphology of the Mesoporous SBA-16 and SBA-15 Materials. *The Journal of Physical Chemistry B* **2006**, *110*, 9183-9187; (b) Fröba, M.; Köhn, R.; Bouffaud, G.; Richard, O.; Van Tendeloo, G., Fe2O3 nanoparticles within mesoporous MCM-48 silica: In situ formation and characterization. *Chemistry of Materials* **1999**, *11*, 2858-2865; (c) Zhao, D.; Feng, J.; Huo, Q.; Melosh, N.; Fredrickson, G. H.; Chmelka, B. F.; Stucky, G. D., Triblock copolymer syntheses of mesoporous silica with periodic 50 to 300 angstrom pores. *Science* **1998**, *279*, 548-552.

5. Knežević, N. Ž.; Durand, J.-O., Large pore mesoporous silica nanomaterials for application in delivery of biomolecules. *Nanoscale* **2015**, *7*, 2199-2209.

6. (a) Benjelloun, M.; Van Der Voort, P.; Cool, P.; Collart, O.; Vansant, E. F., Reproducible synthesis of high quality MCM-48 by extraction and recuperation of the gemini surfactant.

Physical Chemistry Chemical Physics **2001**, *3*, 127-131; (b) Hitz, S.; Prins, R., Influence of Template Extraction on Structure, Activity, and Stability of MCM-41 Catalysts. *Journal of Catalysis* **1997**, *168*, 194-206; (c) Perez, L. L.; Ortiz-Iniesta, M. J.; Zhang, Z.; Agirrezabal-Telleria, I.; Santes, M.; Heeres, H. J.; Melian-Cabrera, I., Detemplation of soft mesoporous silica nanoparticles with structural preservation. *Journal of Materials Chemistry A* **2013**, *1*, 4747-4753.

7. Chen, C.-Y.; Li, H.-X.; Davis, M. E., Studies on mesoporous materials: I. Synthesis and characterization of MCM-41. *Microporous Materials* **1993**, *2*, 17-26.

8. Sumper, M., Biomimetic Patterning of Silica by Long-Chain Polyamines. *Angewandte Chemie International Edition* **2004**, *43*, 2251-2254.

9. Mann, S., *Biomineralization: principles and concepts in bioinorganic materials chemistry*. Oxford University Press on Demand: 2001; Vol. 5.

10. Dickey, F. H., The Preparation of Specific Adsorbents. *Proceedings of the National Academy of Sciences of the United States of America* **1949**, *35*, 227-229.

11. (a) Wei, Y.; Jin, D.; Ding, T.; Shih, W.-H.; Liu, X.; Cheng, S. Z. D.; Fu, Q., A Non-surfactant Templating Route to Mesoporous Silica Materials. *Advanced Materials* **1998**, *10*, 313-316; (b) Wei, Y.; Xu, J.; Dong, H.; Dong, J. H.; Qiu, K.; Jansen-Varnum, S. A., Preparation and Physisorption Characterization of D-Glucose-Templated Mesoporous Silica Sol–Gel Materials. *Chemistry of Materials* **1999**, *11*, 2023-2029.

12. Larsen, G.; Lotero, E.; Marquez, M., Facile Sol-gel Synthesis of Porous Silicas Using Poly(propylene)imine Dendrimers as Templates. *Journal of Materials Research* **2011**, *15*, 1842-1848.

13. (a) Pang, J.-B.; Qiu, K.-Y.; Wei, Y.; Lei, X.-J.; Liu, Z.-F., A facile preparation of transparent and monolithic mesoporous silica materials. *Chemical Communications* **2000**, 477-478; (b) Pang, J. B.; Qiu, K. Y.; Wei, Y., Preparation of mesoporous silica materials with non-surfactant hydroxy-carboxylic acid compounds as templates via sol–gel process. *Journal of Non-Crystalline Solids* **2001**, *283*, 101-108; (c) Pang, J.-B.; Qiu, K.-Y.; Wei, Y., A New Nonsurfactant Pathway to Mesoporous Silica Materials Based on Tartaric Acid in Conjunction with Metallic Chloride. *Chemistry of Materials* **2001**, *13*, 2361-2365; (d) Cheng, S.; Wei, Y.; Feng, Q.; Qiu, K.-Y.; Pang, J.-B.; Jansen, S. A.; Yin, R.; Ong, K., Facile Synthesis of Mesoporous Gold–Silica Nanocomposite Materials via Sol–Gel Process with Nonsurfactant Templates. *Chemistry of Materials* **2003**, *15*, 1560-1566.

14. Zheng, J.-Y.; Pang, J.-B.; Qiu, K.-Y.; Wei, Y., Synthesis of mesoporous silica materials via nonsurfactant templated sol-gel route by using mixture of organic compounds as template. *Journal of sol-gel science and technology* **2002**, *24*, 81-88.

15. Misran, H.; Singh, R.; Yarmo, M. A., Nonsurfactant route of fatty alcohols decomposition for templating of mesoporous silica. *Microporous and Mesoporous Materials* **2008**, *112*, 243-253.

16. Mukherjee, I.; Mylonakis, A.; Guo, Y.; Samuel, S. P.; Li, S.; Wei, R. Y.; Kojtari, A.; Wei, Y., Effect of nonsurfactant template content on the particle size and surface area of monodisperse mesoporous silica nanospheres. *Microporous and Mesoporous Materials* **2009**, *122*, 168-174.

17. Gao, Z.; Zharov, I., Large Pore Mesoporous Silica Nanoparticles by Templating with a Nonsurfactant Molecule, Tannic Acid. *Chemistry of Materials* **2014**, *26*, 2030-2037.

18. (a) Jiang, Y.; Sun, W.; Zhou, L.; Ma, L.; He, Y.; Gao, J., Improved Performance of Lipase Immobilized on Tannic Acid-Templated Mesoporous Silica Nanoparticles. *Applied Biochemistry and Biotechnology* **2016**, *179*, 1155-1169; (b) Gao, J.; Lei, H.; Han, Z.; Shi, Q.; Chen, Y.; Jiang, Y., Dopamine functionalized tannic-acid-templated mesoporous silica nanoparticles as a new sorbent for the efficient removal of Cu2+ from aqueous solution.

Scientific Reports **2017,** *7,* 45215; (c) Sahiner, N.; Sagbas, S.; Aktas, N., Preparation and characterization of monodisperse, mesoporous natural poly(tannic acid)–silica nanoparticle composites with antioxidant properties. *Microporous and Mesoporous Materials* **2016,** *226,* 316-324.

19. Grojo, D.; Boarino, L.; Leo, N. D.; Rocci, R.; Panzarasa, G.; Delaporte, P.; Laus, M.; Sparnacci, K., Size scaling of mesoporous silica membranes produced by nanosphere mediated laser ablation. *Nanotechnology* **2012,** *23,* 485305.

20. Silencieux, F.; Bouchoucha, M.; Mercier, O.; Turgeon, S.; Chevallier, P.; Kleitz, F.; Fortin, M.-A., Mesoporous Silica Nanoparticles under Sintering Conditions: A Quantitative Study. *Langmuir* **2015,** *31,* 13011-13021.

21. Ruggiero, I.; Terracciano, M.; Martucci, N. M.; De Stefano, L.; Migliaccio, N.; Tatè, R.; Rendina, I.; Arcari, P.; Lamberti, A.; Rea, I., Piranha treatment-Diatomite silica nanoparticles for drug delivery. *Nanoscale Research Letters* **2014,** *9,* 329-329.

22. Guinier, A., *X-ray Diffraction in Crystals, Imperfect Crystals, and Amorphous Bodies.* Dover Publications: 1994.

23. Feigin, L. A.; Svergun, D. I., *Structure analysis by small-angle X-ray and neutron scattering.* Springer Science: New York, 1987.

24. (a) Glatter, O., A new method for the evaluation of small-angle scattering data. *Journal of Applied Crystallography* **1977,** *10,* 415-421; (b) Fritz, G.; Bergmann, A.; Glatter, O., Evaluation of small-angle scattering data of charged particles using the generalized indirect Fourier transformation technique. *Journal of Chemical Physics* **2000,** *113,* 9733-9740.

25. Cherny, A. Y.; Anitas, E. M.; Osipov, V. A.; Kuklin, A. I., Scattering from surface fractals in terms of composing mass fractals. *Journal of Applied Crystallography* **2017,** *50,* 919-931.

26. Nishikawa, K., Pore Structure Analyses of Carbons by Small-Angle X-ray Scattering. In *Carbon Alloys,* YASUDA, E.-i.; INAGAKI, M.; KANEKO, K.; ENDO, M.; OYA, A.; TANABE, Y., Eds. Elsevier Science: Oxford, 2003; pp 175-188.

27. Shutava, T.; Prouty, M.; Kommireddy, D.; Lvov, Y., pH Responsive Decomposable Layer-by-Layer Nanofilms and Capsules on the Basis of Tannic Acid. *Macromolecules* **2005,** *38,* 2850-2858.

28. Carcouët, C. C. M. C.; van de Put, M. W. P.; Mezari, B.; Magusin, P. C. M. M.; Laven, J.; Bomans, P. H. H.; Friedrich, H.; Esteves, A. C. C.; Sommerdijk, N. A. J. M.; van Benthem, R. A. T. M.; de With, G., Nucleation and Growth of Monodisperse Silica Nanoparticles. *Nano Letters* **2014,** *14,* 1433-1438.

29. Toth, I. Y.; Szekeres, M.; Turcu, R.; Saringer, S.; Illes, E.; Nesztor, D.; Tombacz, E., Mechanism of in situ surface polymerization of gallic acid in an environmental-inspired preparation of carboxylated core-shell magnetite nanoparticles. *Langmuir* **2014,** *30,* 15451-61.

30. Erdemgil, F. Z.; Şanli, S.; Şanli, N.; Özkan, G.; Barbosa, J.; Guiteras, J.; Beltrán, J. L., Determination of pKa values of some hydroxylated benzoic acids in methanol–water binary mixtures by LC methodology and potentiometry. *Talanta* **2007,** *72,* 489-496.

31. National Center for Biotechnology Information. PubChem Compound Database; CID=8357, https://pubchem.ncbi.nlm.nih.gov/compound/8357 (accessed Oct. 29, 2018).

32. Erdogan, G.; Karadag, R., Quercetin (3, 3', 4', 5, 7-pentahydroxyflavone) Complexes with Calcium (II) and Magnesium (II), Its Potentiometrie and Spectrophotometric studies. *Reviews in Analytical Chemistry* **2005,** *24,* 9-24.